JOURNAL OF SOLID STATE CHEMISTRY 36, 275–288 (1981)

Phase Relations and Exsolution Phenomena in the System NiO–TiO_2

THOMAS ARMBRUSTER*

Institut Für Mineralogie der Ruhr-Universität, D-4630 Bochum, West Germany

Received February 6, 1980; in revised form May 19, 1980

The phase relations in the system NiO–TiO_2 were studied between 1000 and 1600°C using quenched powder specimens, DTA runs, and single crystal diffusion couples. Quenching experiments establish the stable phases TiO_2 (rutile), $NiTiO_3$ an ilmenite structure type, $Ni_{2(1+x)}Ti_{1-x}O_4$ ($x \geq 0.16$), a cation-excess spinel, and $Ni_{1-2x}Ti_xO$ (rocksalt structure type). DTA runs reveal the existence of an additional nonstoichiometric ilmenite phase $Ni_{1-2x}Ti_{1+x}O_3$ ($x \leq 0.03$) above 1260°C. In quenched (1500, 1450°C) or slowly cooled single crystal diffusion couples, mutual oriented exsolutions occur in the rutile crystal and in the ilmenite diffusion zone. Orientation relations are: $\{101\}_{rutile} \| \{11\bar{2}0\}_{ilmenite}$; $\langle 010\rangle_{rutile} \| \langle 00.1\rangle_{ilmenite}$. The cation-excess spinel decomposes below 1375°C into oriented intergrowth of $NiTiO_3$ (ilmenite) and NiO: $\{111\}_{NiO} \| \{0001\}_{NiTiO_3}$; $\langle 110\rangle_{NiO} \| \langle 21.0\rangle_{NiTiO_3}$.

Introduction

Randomly distributed point defects in a crystal structure can migrate to form a superstructure or can gather into single structural complexes only to disappear by ordering to an intermediate phase with a different crystal structure. Such accumulations of defects or formations of intermediate phases have been demonstrated for oxides of transition metals, e.g., niobium, tungsten, molybdenum, rhenium, and titanium. The homologous series Ti_nO_{2n-1}, for instance, can be derived by crystallographic shearings of the nearly close-packed oxygen lattice in rutile. The arrangement of oxygen ions remains almost unaffected, whereas the distribution of octahedrally coordinated cations is changed. With increasing condensation of octahedra (decreasing n), the valence of titanium decreases. Therefore, the so called crystallographic shear structures have their stability range at low oxygen pressures. Substituting Ti^{3+} by Fe^{3+}, V^{3+}, or Cr^{3+} such phases are even stable in air at elevated temperatures. Surprisingly, nothing is reported in the literature about intermediate structures as a consequence of defect accumulations in rutile specimens wherein Ti^{4+} is partially substituted by divalent cations. Diffusion experiments with divalent cations in rutile show a diffusion mechanism along isolated point defects or interstitial positions (*1*). The system NiO–TiO_2 was selected to investigate the existence of intermediate structures or exsolutions in rutile (TiO_2) based on ordering of defects which result from the charge deficiency of divalent cations. The choice was made because Ni^{2+} has a similar ionic radius ($Ni^{(VI)}$: r = 0.070 nm) to Ti^{4+} ($Ti^{(VI)}$: r = 0.0605 nm) (*2*), a high octahedral site preference, and is quite stable with regard to oxidation.

* Present address: Laboratorium für chem. und. miner. Kristallographie Freiestraße 3, CH-3012 Bern, Switzerland.

0022-4596/81/030275-14$02.00/0

Previous Work

The first systematic high-temperature investigation in the system NiO–TiO_2 was carried out by Birnbaum and Scott (*3*), who described $NiTiO_3$ with ilmenite structure ($R\bar{3}$) as the only binary compound. These results were confirmed by the work of different scientists (*4–9*), who used either powdered oxides for high-temperature reactions, or coprecipitated TiO_2 hydrogels and organic Ni^{2+} complexes as precursor phases to maintain higher reactivity. Loshkarev and Sycheva (*7*) concluded from conductivity measurements that at 1350°C up to 3% Ti^{4+} can be dissolved in the p-type semiconductor $Ni_{1-x}O$. Klesheev and Scheinkman (*6*) as well as Satow *et al.* (*10*) could not prove solubility of Ni^{2+} in rutile. Barber and Farabaugh (*11*) observed (001), [100] glide planes in 0.1 mol% NiO-doped rutile single crystals. Zaharescu and Macarovici (*12*) published the first complete phase diagram, which is characterized by a eutectic between rutile and $NiTiO_3$ at 1450°C and 35 wt% NiO and a second eutectic at 1615°C and 60 wt% NiO between $NiTiO_3$ and NiO. Bayer and Flörke (*13*) showed that there is also a phase with spinel structure and they proposed the composition Ni_2TiO_4. Werner and Gebert (*14*) concluded from microprobe analysis of spinel single crystals, grown by diffusion (1500°C), that the composition must be Ni_3TiO_5. Armbruster (*15*) and Laqua *et al.* (*16*) showed that this unusual composition of a spinel phase can be related to an endmember at 1500°C of the hitherto unknown solid solution series $Ni_{2(1+x)}Ti_{1-x}O_4$ (*15*). Shimura and Kawamura (*17*) described a new orthorhombic phase Ni_5TiO_7, which was crystallized by slow cooling in a sodium borate flux. Recently, an improved phase diagram has been published by Laqua *et al.* (*16*) showing the stability range of the solid solutions $Ti_{1-x}Ni_{2x}O_2$ (rutile), $NiTiO_3$ (ilmenite), and $Ni_{1-z}Ti_{z/2}O$ (rocksalt-spinel type) on the NiO-TiO_2 join (Fig. 1). Melting of $NiTiO_3$ was observed at 1530°C in the NiO-poor region and at 1580°C in the NiO-rich region of the phase diagram.

Experimental

a. Powder Experiments

To reinvestigate the NiO–TiO_2 phase diagram, mixtures of powdered oxides NiO (Baker 1153) and TiO_2 (Kronos R-1053) were homogenized by grinding under acetone in an agate ball mill, pressed to tablets, prereacted 24 hr at 1000°C, again homogenized, and finally pressed to discs. Samples were prepared with compositions varying in steps of 5 mol%. The time-consuming preparation procedure was necessary to obtain equilibrium conditions for the high-temperature treatment. Fractions of the samples were quenched in water after equilibrating 24 hr up to 1 week at selected temperatures in a vertical rhodium-wound furnace. The temperature was controlled by an EL-18 thermocouple. Quenching was carried out by releasing a platinum wire on which a platinum sieve containing the sample was fixed, so that the sample was dropped through the bottom of the vertical tube, where it was rapidly quenched in

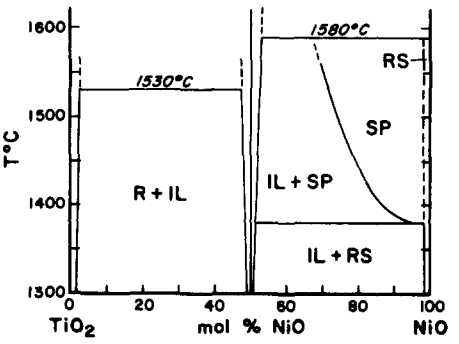

FIG. 1. Improved phase diagram NiO–TiO_2 according to Laqua *et al.* (*16*). R, Rutile; IL, ilmenite; SP, spinel; RS, rocksalt structure NiO.

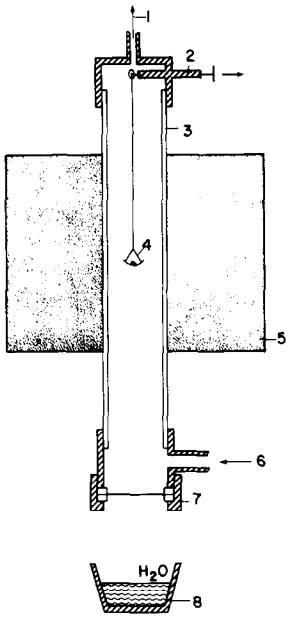

FIG. 2. Cross-sectional view through the furnace and the quenching device constructed for the reinvestigation of the phase diagram. (1) Gas outlet; (2) quenching device (brass), pulling the handle unhooks the sample; (3) alumina tube; (4) platinum sieve with sample; (5) furnace; (6) gas inlet; (7) aluminum foil held between two Teflon gaskets and fastened with a brass screw-ring; (8) water beaker.

water (Fig. 2). To prevent partial high-temperature reduction of Ti^{4+}, the reaction tube was continuously flushed by oxygen. DTG runs indicated that Ni^{2+} will not be oxidized under those conditions. The phases present after high-temperature treatment were identified using X-ray diffraction (Huber-Guinier type camera, Cu$K\alpha_1$ radiation, silicon as internal standard). Cell dimensions were refined with reflections between 25 and 95° 2 θ. Film intensities were measured with a photometer. High-temperature Guinier photographs (Enraf-Nonius camera, Cu$K\alpha$ radiation) were taken from selected powder mixtures.

Exsolutions and grain size were checked by optical microscopy using polarized, reflected light for air and oil immersion. From all prereacted (1000°C) powder mixtures, DTA/DTG runs were carried out using a Mettler instrument with a cooling and heating rate of 5°C/min and 10°C/min, respectively. In order to prove stoichiometry selected samples were analyzed by electron microprobe.

b. Single Crystal Growth

To verify the existence of the phase Ni_5TiO_7 described by Shimura and Kawamura (*17*), single crystal synthesis by slow cooling in a sodium borate flux was used. Composition of the crystals was determined by standard chemical methods for Ni, Ti, B, and Na. Single crystals of the spinel phase in the system NiO–TiO_2 were grown by a diffusion method according to Flörke, as described by Werner and Gebert (*14*). Fractions of rutile single crystals or powder tablets were placed in a NiO powder bed, annealed 4 weeks at 1450 or 1500°C, respectively, and subsequently quenched by water. NiO single crystals (20 × 5 × 5 mm) were grown using the horizontal floating zone technique by Saurat and Revcolevschi (*18*).

c. Diffusion Experiments

Zone molten NiO single crystals and verneuil grown rutiles (Lindes Corp., New York) were used for diffusion runs. NiO (3 × 3 × 3 mm) and TiO_2 (6 × 6 × 6 mm) single crystals were held, with finely polished faces in contact, by a platinum wire. The original boundary between the different-sized single crystals acts as a marker in determining the direction of diffusion. Rutile single crystal boules were oriented parallel (001), (110), and (100) within an angular deviation of ±2°. Orientation of rutile was maintained following the favored natural cleavability along (110) and monitored by the X-ray Laue backreflection method. For studies of the diffusion profile by scanning electron microscopy, both crystals were cut into cubes and polished on all faces, then fastened together in such

a way that the reaction zone could be observed parallel as well as perpendicular to the direction of diffusion. Single crystal diffusion experiments were performed in duplicate at 1450 and 1500°C under a neutral atmosphere. One single crystal couple was quenched by water while the other was slowly cooled down with the furnace. The high-temperature heating time was 3 and 6 weeks. Fractions of the specimen were analyzed by the X-ray precession method (Ni-filtered Cu$K\alpha$ radiation), reflected light microscopy, scanning electron microscopy, and electron microprobe.

Results

Quenching experiments between 1000 and 1600°C establish the stability ranges of the phases TiO_2 (rutile), $NiTiO_3$ (ilmenite type), $Ni_{2(1+x)}Ti_{1-x}O_4$ ($x \geqq 0.16$), a nonstoichiometric spinel phase classified as cation-excess spinel, and $Ni_{1-2x}Ti_xO$ ($x \leqq 0.02$), a rocksalt structure-type. Melting of the ilmenite phase occurred at 1520°C in the rutile–ilmenite assemblage and at 1560°C in the spinel–ilmenite stability field. Those powder qenching results compare favorably with those obtained by Laqua *et al.* (*16*). Additional, hitherto unknown information about a second ilmenite phase is evident from DTA measurements and single crystal diffusion couples.

High and Low Ilmenite

DTA/DTG heating experiments of ilmenite-type-containing samples reveal a sharp endothermic DTA peak at 1260 ± 10°C without any weight change of the samples. Cooling of these specimens from 1500°C results in an exothermic DTA peak at 1280 ± 10°C. Such DTA curves, where the heating peak occurs at lower temperatures than the cooling peak, cannot be explained by simple phase transformations without change of stoichiometry. Even displacive transformations show a normal hysteresis. Neither by optical investigation of samples quenched from 1000, 1200, 1450, and 1550°C, respectively, with the bulk composition $NiTiO_3$, nor by unit cell refinements, could any structural change be confirmed. Independent of the quenching temperature, all $NiTiO_3$ powder specimens show the same cell dimensions ($a_0 = 0.5031$ (1) nm, $c_0 = 1.3785$ (2) nm)[1]. However, X-ray powder reflections obtained from samples quenched from 1450 and 1550°C become diffuse (Table I). High-temperature Guinier photographs of $NiTiO_3$ samples exhibit a slight increase in slope of the thermal expansion curve above 1260°C. Nevertheless, this discontinuity is not significant. Because of the permissible load of the heating element, measurements were possible only up to 1350°C. In all cases X-ray reflections were consistent with space group $R\bar{3}$. As demonstrated later by single crystal diffusion experiments, these results can be understood only if there is a nonstoichiometric phase $Ni_{1-2x}Ti_{1+x}O_3$ or two submicroscopically intergrown phases above 1260°C (called high-ilmenite), with a structure very similar to the ilmenite phase below 1260°C (low-ilmenite). The low- to high-ilmenite transition and vice versa, respectively, must be accompanied by an exsolution of a further phase, hitherto not detected by X-ray powder techniques.

Spinel Solid Solution

The formation of a spinel phase in the system NiO–TiO_2 is connected with an endothermic DTA heating effect at 1375 ± 10°C without any weight change, so that reduction or oxidation must be excluded. At 1375°C the DTA effect which is characteristic of spinel formation increases sharply and then shows a flat shoulder until saturation of the solid solution is reached.

[1] Standard deviations are given in parentheses and refer to the last digit.

TABLE I

d-VALUES (nm) AND X-RAY POWDER INTENSITIES OF THE ILMENITE PHASES ($R\bar{3}$) IN THE SYSTEM NiO–TiO_2

	Low-ilmenite				High-ilmenite			
	Tempered at 1000°C		Tempered at 1550°C + retempered at 900°C		Quenched from 1450°C		Quenched from 1550°C	
h k l	*d*(nm)	I/I_1	*d*(nm)	I/I_1	*d*(nm)	I/I_1	*d*(nm)	I/I_1
0 1 2	0.368	50	0.368	52	0.368	45	0.368	47
1 0 4	0.2704	100	0.2704	100	0.2702	100	0.2703	100
1 1 0	0.2517	85	0.2517	84	0.2516	71	0.2515	70
1 1 3	0.2206	40	0.2207	40	0.2208	35	0.2206	25
2 0 2	0.2077	<2	0.2078	<2				
0 2 4	0.1841	42	0.1841	42	0.1841	38	0.1842	29
1 1 6	0.1697	60	0.1696	61	0.1696	48	0.1696	47
1 2 2	0.1602	10	0.1602	9	0.1602	9	0.1601	9
2 1 4	0.1486	32	0.1486	32	0.1486	22	0.1486	25
0 3 0	0.1452	38	0.1452	38	0.1452	27	0.1452	22
1 0 10	0.1314	9	0.1315	10	0.1315	3	0.1315	3
2 2 0	0.1258	10	0.1258	11	Diffuse		Diffuse	
0 3 6	0.1228	<2	0.1228	<2	Diffuse		Diffuse	
2 2 3	0.1213	<2	0.1213	<2	Diffuse		Diffuse	
1 2 8	0.1190	10	0.1191	10	Diffuse		Diffuse	
1 3 4	0.1141	10	0.1141	10	Diffuse		Diffuse	
2 2 6	0.1103	10	0.1104	10	Diffuse		Diffuse	
2 1 10	0.1057	14	0.1057	13	Diffuse		Diffuse	
4 0 4	0.1039	16	0.1039	16	Diffuse		Diffuse	
	a_0 = 0.5031 (1) nm c_0 = 1.3785 (2) nm				a_0 = 0.5030 (1) nm c_0 = 1.3786 (2) nm			

The following spinel compositions, which are Ti^{4+}-saturated members of the solid series, were determined by electron microprobe:

1400°C: $Ni_{3.28}Ti_{0.36}O_4$
1500°C: $Ni_{2.40}Ti_{0.80}O_4$
1550°C: $Ni_{2.32}Ti_{0.84}O_4$

The stoichiometric spinel composition Ni_2TiO_4 could not be obtained within the solidus range. Finely ground spinels are grey-green colored and cannot be distinguished from pure NiO. Unit cell dimensions refined from Guinier photographs (space group $Fd3m$) show a slight increase with decreasing Ti^{4+} concentration (Table II). Extrapolation to NiO yields a cell dimension of 0.8348 nm which agrees well with the double cell of NiO in the space group $Fm3m$. Extrapolation to the hypothetical composition Ni_2TiO_4 results in 0.8340 nm. Slow cooling of the cation-excess spinels or retempering below 1375°C causes decomposition of the spinel structure:

$$Ni_{2(1+x)}Ti_{1-x}O_4 \rightarrow (3x + 1)\ NiO + (1 - x)\ NiTiO_3$$

Optical study of decomposed samples reveals lamellar or tabular exsolutions along four directions in a randomly cut mother crystal. Precession photographs indicate that $NiTiO_3$ (ilmenite) and NiO (rocksalt

TABLE II

d-VALUES AND X-RAY POWDER INTENSITIES OF THE SPINEL PHASE ($Fd3m$) $Ni_{2(1+x)}Ti_{1-x}O_4$

	$Ni_{2.4}Ti_{0.8}O_4$		$Ni_{2.67}Ti_{0.67}O_4$		$Ni_{3.27}Ti_{0.36}O_4$		$Ni_{3.62}Ti_{0.19}O_4$		NiO ASTM 4-835	
h k l	*d* (nm)	I/I_1	*d* (nm)	I/I_1	*d* (nm)	I/I_1	*d* (nm)	I/I_1	*d* (nm)	I/I_1
1 1 1	0.4817	30	0.4820	28	0.4828	11	0.4828	5	—	—
2 2 0	0.2949	39	0.2950	33	0.2952	11	0.2953	6	—	—
3 1 1	0.2513	100	0.2514	88	0.2516	40	0.2517	19	—	—
2 2 2	0.2408	35	0.2410	62	0.2407	82	0.2410	87	0.2410	91
4 0 0	0.2086	62	0.2085	100	0.2085	100	0.2087	100	0.2088	100
3 3 1	0.1914	2	0.1915	4	—	—	—	—	—	—
4 2 2	0.1703	15	0.1702	14	0.1703	<1	0.1704	<1	—	—
5 1 1	0.1606	45	0.1606	28	0.1606	15	0.1606	9	—	—
4 4 0	0.1475	65	0.1475	79	0.1475	68	0.1475	49	0.1476	57
5 3 1	0.1410	<1	0.1410	<1	—	—	—	—	—	—
6 2 0	0.13189	4	0.13187	3	0.13204	<1	0.13197	<1	—	—
5 3 3	0.12722	11	0.12722	11	0.12728	<1	0.12725	<1	—	—
6 2 2	0.12574	12	0.12577	26	0.12582	34	0.12584	30	0.1259	16
4 4 4	0.12038	12	0.12041	37	0.12047	27	0.12045	19	0.1206	13
6 4 2	0.11149	[a]	0.11151	[a]	0.11149	[a]	0.11156	[a]	—	—
7 3 1	0.10862	[a]	0.10863	[a]	0.10869	[a]	0.10868	[a]	—	—
	25% TiO_2		20% TiO_2		10% TiO_2		5% TiO_2		0% TiO_2	
I_{220}/I_{440}	0.60		0.42		0.16		0.12		0	
a_0 (nm)	0.8342 (1)		0.8343 (1)		0.8346 (1)		0.8347 (1)		0.835	

[a] Intensity not measured.

type) are mutually oriented (Fig. 3) obeying the law:

$$\{111\}_{NiO} \| \{0001\}_{NiTiO_3};$$
$$\langle 110\rangle_{NiO} \| \langle 21.0\rangle_{NiTiO_3}.$$

Associated with this exsolution is a symmetric, sharp exothermic peak in DTA-cooling experiments. Such peaks show a characteristic hysteresis according to the saturation temperature of the spinel solid solution. The decomposition temperature also depends on the grain size of the spinel starting material. When retempering originally quenched spinel samples at 1260°C in a high-temperature Guinier camera, no additional X-ray reflections other than of ilmenite ($NiTiO_3$), the rocksalt structure type (NiO), and spinel could be found. It seems likely that ilmenite nuclei arise in the spinel lattice by crystallographic shearing along the close packed oxygen layers contemporaneously with cation diffusion proposed by Kachi *et al.* (*19*). All X-ray spinel powder patterns could be indexed in the space group $Fd3m$. Intensity measurements of the powder diffraction lines as a function of increasing Ti^{4+} content show a significant increase in the intensities which result from doubling the NiO ($Fm3m$) cell dimensions. However, reflections of the type Okl: $(k, l) = 2n$ (hOl: $(h, l) = 2n$, hkO: $(h, k) = 2n$) obey the additional limitation $k + l = 4n$ ($h + l = 4n$, $h + k = 4n$). The characteristic difference between the spinel- and the rocksalt-type (NiO) consists in occupation of tetrahedral sites and the creation of octahedral vacancies in the spinel. Two-thirds of the cations in the spinel-type are ordered on octahedral and one-third on tetrahedral sites, whereas in the rocksalt-type all octahedra but no tetra-

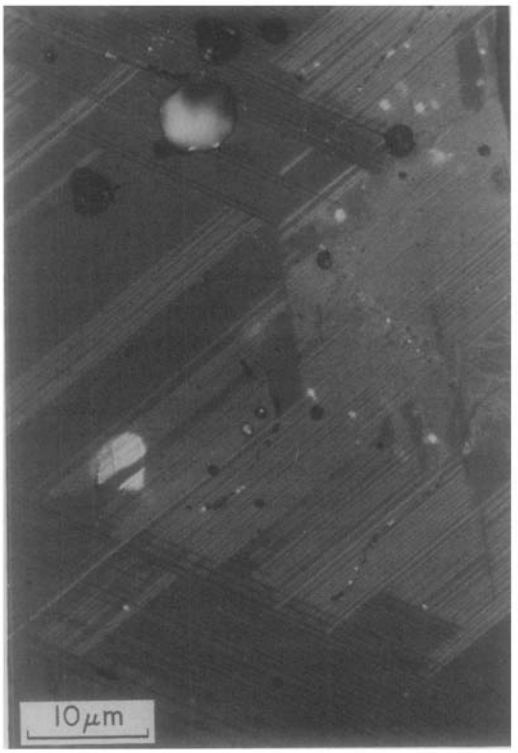

FIG. 3. Decomposed spinel sample due to retempering of a spinel at 1250°C. Oriented $NiTiO_3$ exsolution lamellae are intergrown with NiO. The NiO host crystal is cut nearly parallel {111} (reflected light photograph using polarized light and oil immersion).

hedra are occupied in a cubic close-packed lattice of oxygen ions. In the $Ni_{2(1+x)}Ti_{1-x}O_4$ cation-excess spinels, additional sites must be occupied. In this case there are not only 24 cations in a spinel unit cell ($Fd3m$) like in a stoichiometric spinel but $24 + 8x$ cations. To evaluate the cation distribution in spinels, a simple method (*20*) which uses the powder intensity ratio of the (220)/(440) lines was adapted to the non-stoichiometric $Ni_{2(1+x)}Ti_{1-x}O_4$ spinels. The (220)-intensity is independent of the occupation of octahedral coordinated cation positions in $Fd3m$ (16 d and 16 c (*21*)). Therefore the (220)-intensity is related to the occupancy of tetrahedral sites (8 a and 8 b), whereas the intensity (440) depends on *all* cation positions of a spinel and can be used as a unit of reference. Inspection of Table II indicates that with increasing Ti^{4+} concentration the (220)/(440) intensity ratio increases. Even if it is evident that with increasing Ti^{4+} content more tetrahedra are occupied, it still remains questionable if Ni^{2+} or Ti^{4+} possesses tetrahedral coordination. In the literature there is only one example, where Ti^{4+} occupies some tetrahedral sites in a spinel: $Ni_{1+x}Fe_{2(1-x)}Ti_xO_4$ (*22, 23*). Examples for Ni^{2+} in tetrahedral coordination in a spinel are $NiCr_2O_4$ and $NiAl_2O_4$ (*24, 25*).

Below 1375°C less than 2 mol% Ti^{4+} can be dissolved in the rocksalt structure of NiO. One Ti^{4+} ion substitutes for two Ni^{2+} ions on octahedral sites with the creation of one octahedral vacancy. X-Ray powder diagrams of such solid solutions $Ni_{1-2x}Ti_xO$ ($x \leqq 0.02$) can be indexed in the space group $Fm3m$. Above 1375°C more than 2 mol% Ti^{4+} can occur in a cubic close packing of oxygen ions; as a result, the rocksalt structure type is changed into a cation-excess spinel. Substitution of two Ni^{2+} by one Ti^{4+} is accompanied with occupancy of one tetrahedron and creation of two octahedral vacancies. This substitition is continued until a saturation composition is reached which is specific for different temperatures. In $Ni_{2.4}Ti_{0.8}O_4$, the saturation composition for 1500°C, 6.4 cations are assumed to be distributed on 16 possible tetrahedral sites (8 a and 8 b), while 19.2 cations are distributed on 32 available octahedral positions (16 c and 16 d) per unit cell ($Fm3m$). It is obvious that additional cations in those spinels will prefer a special order to prevent deformational stress. Even single crystal structure refinements, currently in progress, cannot clear the coordination of Ni^{2+} and Ti^{4+} in $Ni_{2(1+x)}Ti_{1-x}O_4$ spinels. The similarity in X-ray scattering behavior makes it impossible to refine exact cation distribution.

"Ni_5TiO_7"

An orthorhombic phase Ni_5TiO_7 suggested by Shimura and Kawamura (*17*) has no stability range in the system NiO–TiO_2. Chemical analyses indicate that this compound is not even a binary phase as asserted (*17*). It seems that the hypothetical Ni_5TiO_7 is identical with the green nickel titane borate reported by Marnier and Bolfa (*26*) when applying a flux of similar composition. Our chemical analyses of crystals with *d*-values conforming to "Ni_5TiO_7" (*17*) reveal the composition $Ni_{4.2}Ti_{0.88}B_{1.5}Na_{0.02}O_7$ (calculated on the basis of 7 oxygen ions).

Diffusion Experiments

Single crystal diffusion experiments were performed to investigate the succession of different phases, solid solution range, exsolution phenomena, and diffusion mechanisms. No attempt was made to describe mutual cation diffusion by physical chemical calculations. In the foreground of this study stood the investigation of structural coherency relations of diffusively grown phases.

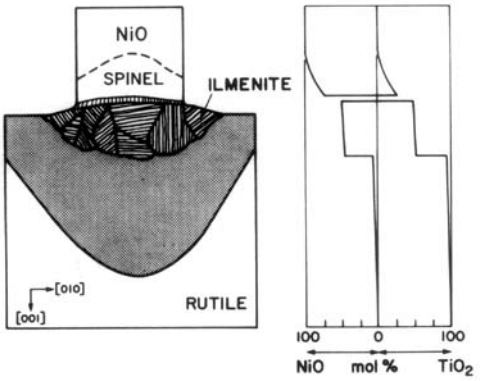

FIG. 4. Left: Cut through a NiO–TiO_2 single crystal diffusion profile, sample quenched from 1450°C. The shaded area in rutile shows the range where Ni-rich exsolutions were found. Right: Microprobe scans over such a diffusion profile cannot discern such small inclusions but provide an average analysis.

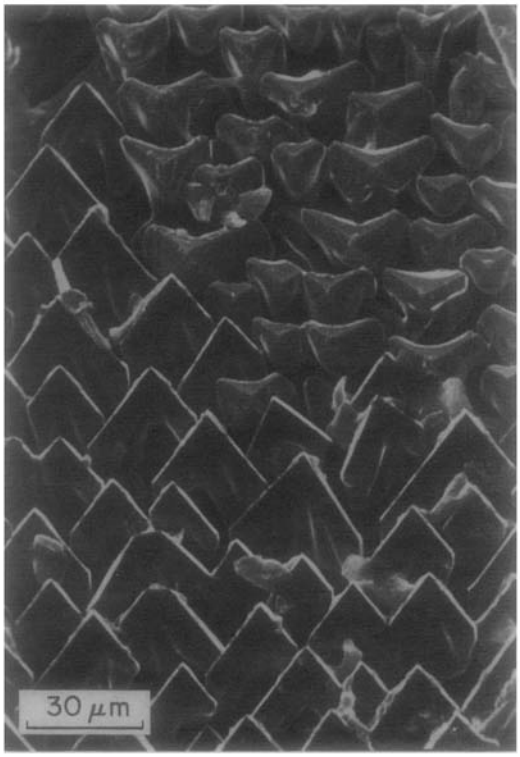

FIG. 5. Epitaxial grown $NiTiO_3$ crystals on the $NiTiO_3$ diffusion zone (SEM photograph).

In the system NiO–TiO_2, the succession of phases—rocksalt-, spinel-, ilmenite-, and rutile-type—was observed in all samples quenched from 1450 and 1500°C (Fig. 4). It is striking that in all runs, independent of the orientation of the rutile crystal, no mechanical or even structural coherency could be found between the spinel- and ilmenite-type areas, although both structures relate to a close packing of oxygen ions. A tiny hollow between both phases, observed in all specimens, is filled with epitaxial ilmenite crystals grown on the ilmenite diffusion zone (Fig. 5). In contrast to that a monocrystalline spinel body is welded to the NiO single crystal without any visible phase boundary. Electron microprobe scans indicate that the Ti^{4+} concentration decreases continuously in the NiO single crystal (Fig. 4). The ilmenite

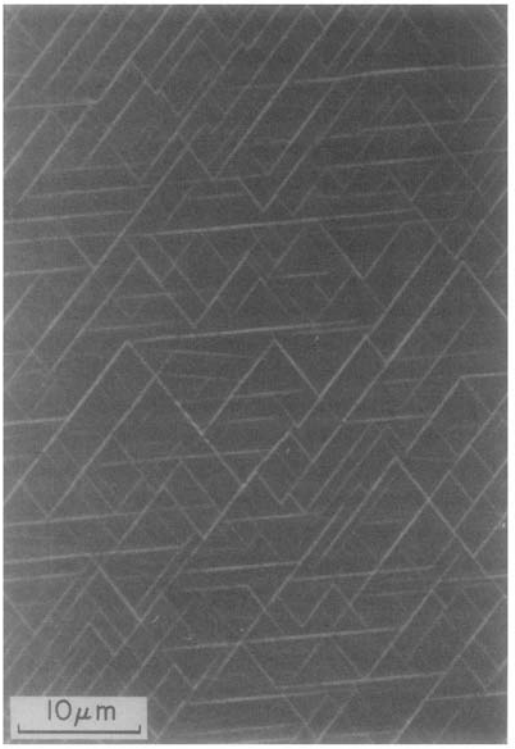

FIG. 6. Titanium-rich exsolutions in the randomly oriented $NiTiO_3$ diffusion zone, specimen quenched from 1450°C (microscopic photograph using polarized light and oil immersion).

phase, which consists mostly of more than one cracked crystal individual, is penetrated in the rutile mother crystal. Frequent cracks in the ilmenite grains may arise from tensions of the volume difference and the varied thermal expansion of rutile and ilmenite. Electron microprobe scans over the diffusion profile indicate that neither the ilmenite nor the rutile zone is homogeneous even if rapidly quenched in water (Fig. 6). In rutile, lamellar or tabular exsolutions of a nickel-rich phase developed in preferred orientation to the rutile host crystal. Quantitative analysis of the exsolved bodies was not possible, because the lamellae are less than 0.1 μm thick. The amount of the exsolution lamellae increases toward the ilmenite zone. Mutually oriented titanium-rich lamellae in the ilmenite diffusion zone occur along the whole profile but increase in frequency toward the rutile host crystal (Fig. 7). Slowly cooled samples have fewer and shorter exsolution lamellae which are broader and more lense shaped compared to those in the quenched specimens. This phenomenon is well known and is in agreement with the tendency of a body to minimize the surface energy. Also these broadened lamellae are still too small for analysis by electron microprobe (< 1 μm). Further retempering at 1200°C yields large, rounded exsolution bodies in rutile which could now be analyzed as stoichiometric $NiTiO_3$ and lamellar exsolutions in ilmenite which were identified as TiO_2-rutile. It remains questionable if these phases are identical with the pretempered phases.

The distribution of the nickel-rich lamellae in rutile describes an ellipsoid, strongly elongated along the rutile *c* axis, but the ilmenite diffusion zone within the rutile mother crystal displays a much smaller preferred anisotropy along the rutile's *c* axis. The contact between the ilmenite-diffusion zone and rutile shows a notched shape (Fig. 8), the ilmenite zone displaying toothlike branches, which may be identical with the exsolutions in the rutile. At high magnifications of the scanning electron microscope, such precursor exsolutions often decorate dislocations by accumulations of lamellae showing different preferred orientations around the two-dimensional crystal defects (Figs. 9 and 10). The titanium-rich lamellae in the ilmenite zone are regularly

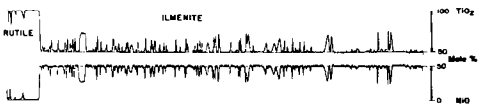

FIG. 7. Electron microprobe scan over a $NiTiO_3$ diffusion profile. The sample was tempered 4 weeks at 1450°C and then slowly annealed with the furnace. Ti-rich exsolutions in ilmenite and Ni-rich exsolutions in rutile are still too small for an accurate microprobe analysis.

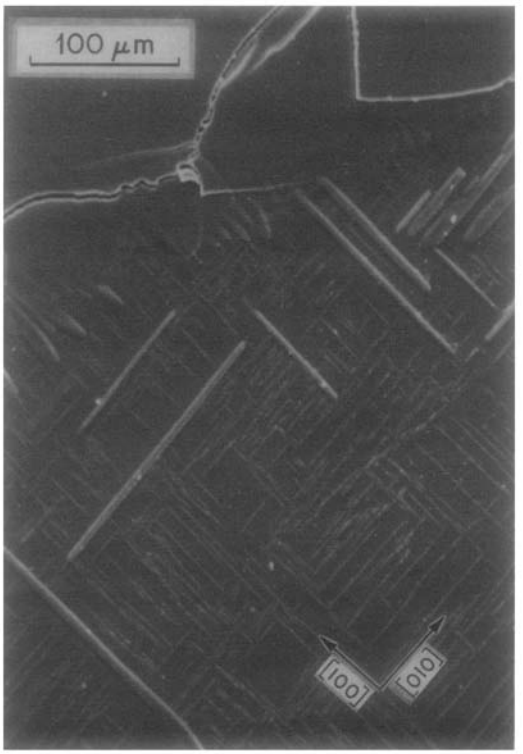

FIG. 8. Contact between the $NiTiO_3$ diffusion zone and the rutile host crystal, sample quenched from 1450°C. The $NiTiO_3$ diffusion zone invades the rutile crystal with toothlike branches (SEM photograph).

distributed and show no decoration effects. Fragments of the ilmenite-zone and the TiO_2-host crystals, cut out from the diffusion couple, show the following orientations (Fig. 11):

$$\{101\}_{\text{rutile}} || \{11\bar{2}0\}_{\text{ilmenite}};$$
$$\langle 010\rangle_{\text{rutile}} || \langle 00.1\rangle_{\text{ilmenite}}.$$

These orientations seem independent of the orientation of the original plane of contact (Fig. 11). The ilmenite lamellae in rutile are oriented with their long axis in {301} in rutile, so that the orientation relation can also be expressed as:

$$\{301\}_{\text{rutile}} || \{1\bar{1}00\}_{\text{ilmenite}};$$
$$\langle 010\rangle_{\text{rutile}} || \langle 00.1\rangle_{\text{ilmenite}},$$

which is identical with the relation given above, because the planes {101} and {301} in rutile cross under an angle of 30°.

The oriented rutile exsolutions in ilmenite form six groups of nonparallel oriented lamellae $\langle 00.1\rangle_{\text{ilmenite}} || \langle 00.1\rangle_{\text{rutile}}$ twinned along {101} and {301}, so that a dense network results. Such a structure of rutile exsolutions, called sagenite ($\dot{\eta}\sigma\alpha\lambda\dot{\eta}\nu\eta$ = the net), is a well-known type of natural rutile, in hematite- or ilmenite-type intergrowth.

In contrast to these orientation relations, no mutual orientation relation was found between the crystals of the ilmenite diffusion zone and the adjoining rutile mother crystal.

Discussion and Conclusions

The diffusion profile obtained (Fig. 4) shows that nickel and titanium diffuse in opposite directions. The well-known preference of a gas transport mechanism for NiO (*16, 27*) causes a gap between the NiO-spinel block and the ilmenite reaction zone which enters deeply into the rutile host. Consequently, between NiO and ilmenite, titanium has to diffuse over the gas phase into the NiO-crystal to form the spinel. The close coherency between the ilmenite zone and the rutile host makes a solid state mechanism between those phases probable. Wittke (*1*) reported that in his diffusion experiments at 1200°C Ni^{2+} does not occupy Ti^{4+} equivalent positions in the rutile structure but diffuses along octahedral interstitial positions which form channels along the rutile *c* axis. Therefore this interstitial diffusion mechanism has been called a "pipe" or "chimney" diffusion (*28, 29*). In contrast to this strongly unisotropic mechanism for the Ni^{2+} diffusion in rutile, titanium migrates along cation vacancies in rutile and has no interstitial-site residence. Consequently, it has similar diffusion rates, as measured and calculated (*30*), for the *a* and *c* directions in

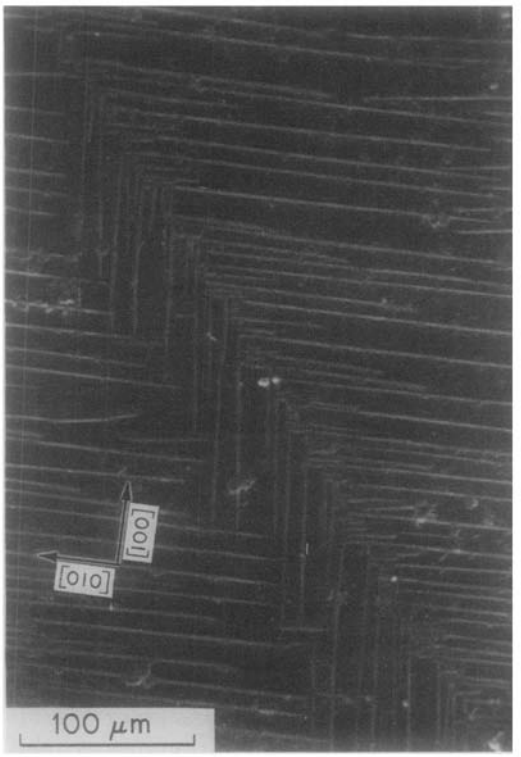

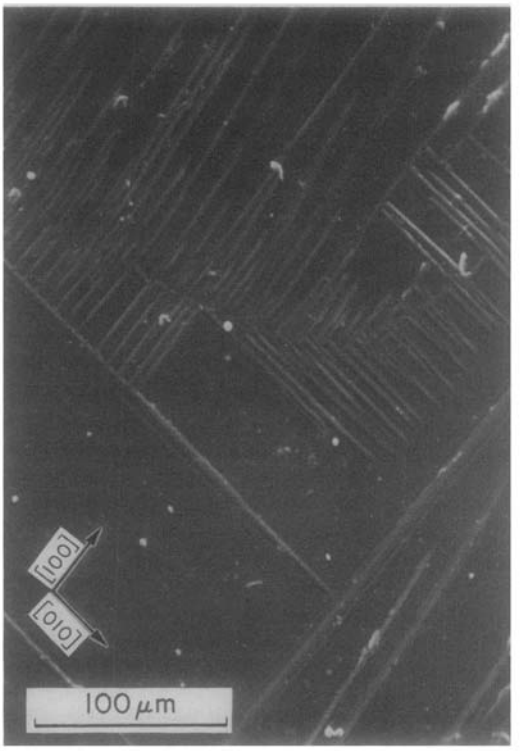

FIGS. 9 AND 10. Nickel-rich exsolutions in the rutile host crystal decorating preexisting dislocations (SEM photograph).

rutile. Flörke and Lee (*31*) demonstrated for Cr^{3+} diffusion in rutile that two-dimensional corundum-structured defects are created around the chimneys of interstitial sites. On the basis of this knowledge, the following model for the diffusion of Ni^{2+} in rutile seems likely: Ni^{2+} invades the rutile host crystal anisotropically along the pipes parallel to the c axis. Accumulation of interstitial Ni^{2+} ions results in defects act-

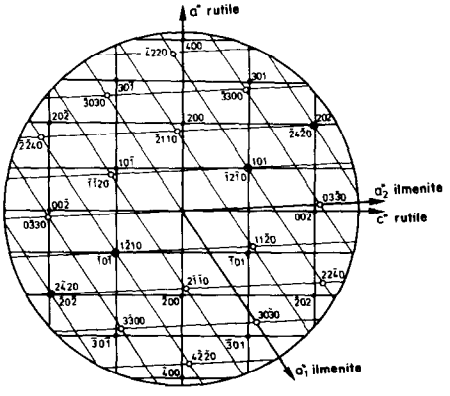

FIG. 11. Zero layer and reciprocal lattice perpendicular {010} rutile and {0001} ilmenite according to the determined orientation relation.

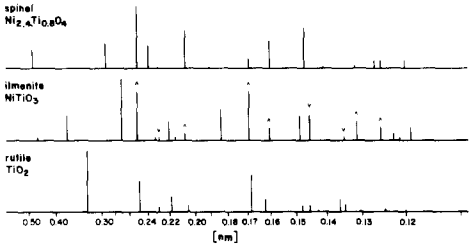

FIG. 12. Schematical diagram of X-ray powder diffraction lines for compounds in the system NiO–TiO_2. Possible coincidences are marked by arrows.

ing as corundum or ilmenite nuclei, respectively, and ilmenite-structured exsolutions grow in rutile. Contrary to expectations, the growth of the $NiTiO_3$ diffusion zone does not follow the same degree of anisotropy as for Ni^{2+} diffusion. The shape of the $NiTiO_3$ zone indicates only a considerably smaller tendency to favor growth along rutile's *c* axis than one might expect from the distribution of the $NiTiO_3$ precursor exsolutions in rutile. The reasons are different mechanisms for the formation of the ilmenite diffusion zone on the one hand and the precursor exsolutions in rutile on the other hand.

Formation of Exsolution Lamellae in Rutile

Ni^{2+} diffuses along the interstitial positions in rutile. Therefore a surplus of positive charges arises which can be balanced either by adjoining additional oxygen ions or by crystallographic shearing of the almost close-packed oxygen layers in rutile, in a way that charge balance is obtained by changing the arrangements of coordination polyhedra. Such mechanism is also known for the formation of the so called Magnéli–Andersson phases which can be derived from the rutile by combined crystallographic shearing along {011} and {121} (*32*). The dense distribution of nickel-rich lamellae in rutile and the notched branches of the $NiTiO_3$ diffusion zone (Fig. 8) make it evident that, due to anisotropic Ni^{2+} diffusion in rutile, Ni^{2+} saturation in TiO_2 is exceeded whereupon shear or dislocation systems originate along preexisting defects in rutile (Figs. 9 and 10). These defects, the favored diffusion paths for Ni^{2+}, cross the rutile host crystal as arched planes often decorated by fish bone-like arrangements of exsolution lamellae. The differences between the uniform orientation of such exsolution lamellae on one side versus that on the other side of the defect may be explained by tensions of the neighboring structure blocks.

Formation of the Ilmenite Diffusion Zone

The rutile mother crystal is intensively destroyed by such precursor exsolutions as those discussed above. In rutile, exsolutions can be oriented parallel to one or more of the equivalent planes: (301), ($\bar{3}$01), (031), and (0$\bar{3}$1). Rotated 60° around the *c* axis, the oxygen frame work remains unchanged whereas nonhexagonal distribution of cations results in four further possible orientations. The growth rate of the block-like $NiTiO_3$ reaction zone mainly depends therefore on the orientation of the precursor exsolutions and on the direction of shear and dislocation systems; consequently the growth rate observed is not consonant with a simple diffusion mechanism in an ideal rutile. It remains questionable to what extent such precursor exsolutions arise during the diffusion process and during the quenching period. But the existence of the big notched branches of the ilmenite diffusion zone (Fig. 8) indicates that these lamellae at least grow before quenching. These problems reveal that it is impossible to answer the question of the Ni^{2+} solubility in TiO_2 (rutile). The discussion of exsolution mechanisms demonstrated that already at this point the limit of the classic phase definition was exceeded. Therefore one cannot estimate the composition below which a nickel-containing rutile solid solution will exist nor at what nickel content two phases must be considered. The Ni^{2+} concentration between the exsolution lamellae in rutile of slowly anealed single crystal diffusion couples was measured with 0.002 mol%, which is below the significance of the electron microprobe. The lack of structural coherency between the rutile mother crystal and the polycrystalline ilmenite zone can be understood by assuming the following facts. There are

eight differently orientated precursor exsolutions in rutile, each competing to grow. As a consequence of a nucleus selection, the small lamellae dissolve whereas the bigger lamellae grow. However, when the reaction zone, invading the rutile crystal, encounters large monocrystalline blocks, those precursor exsolutions which do not match the orientation of the reaction zone are dissolved or rearranged. Additional orientations of single crystal blocks can occur which may be considered as an average orientation arising from several precursor lamellae. Further distortion of single crystal blocks in the reaction zone can be produced by different creep processes during sintering.

Exsolution Lamellae in Ilmenite

Powder and single crystal experiments indicate that there must be a connection between the exsolutions in ilmenite and the observed DTA heating effect at 1260°C and the DTA cooling effect 1280°C, respectively, which occur in all ilmenite containing samples without any weight change. These phenomena can be explained only if, above 1260°C, a titanium-rich ilmenite exists consisting of 51–56 mol% TiO_2 as calculated from microprobe scans over the ilmenite diffusion profile. The titanium content of this nonstoichiometric high-ilmenite is a function of the temperature. When heated above 1260°C the ilmenite becomes enriched in titanium. The DTA cooling effect at 1275°C indicated the beginning of the exsolution process; below 1260°C only a stoichiometric $NiTiO_3$, called low-ilmenite, is stable. From a thermodynamic point of view, high- and low-ilmenite should be considered as two phases because the DTA experiments reveal a defined transition temperature between both ilmenites. Nevertheless, additional work is necessary to understand the structural relations between both phases. The existence of titanium-rich exsolutions even in quenched samples, which after slowly annealing or retempering consist of rutile, indicates a high structural coherency between host and guest phase which will be discussed in a further paper. Laqua *et al.* (*16*) did not find any exsolutions in their quenched NiO–TiO_2 powder specimen and asserted an ilmenite solid solution range of 48–52 mol% TiO_2 at 1408°C analyzed by electron microprobe using polycrystalline sinter tablets as calibration standards. The ilmenite composition was reported to be associated with a variation of the ilmenite c_0 cell dimension. They (*16*) measured c_0 for ilmenite to be 1.377 nm in the ilmenite-rutile phase assemblage (quenched from 1408°C), 1.380 nm in the ilmenite homogeneity range, and 1.383 nm in the spinel-ilmenite assemblage. Own results contradict these observations: (1) electron microprobe analysis, using NiO and TiO_2 single crystals as calibration standards, show no nickel-rich ilmenite. (2) In the whole ilmenite diffusion profile, titanium-rich exsolution were found (Fig. 8). (3) No change of the ilmenite cell dimensions could be measured using a Huber–Guinier camera ($CuK\alpha_1$) which has a significant better resolution than the camera applied by Laqua *et al.* (*16*). It seems likely that Laqua *et al.* calculated larger cell dimensions in the spinel-ilmenite phase assemblage because of coincidence of ilmenite and spinel powder reflections and smaller c_0 values in the rutile-ilmenite phase assemblage for the same reason, respectively. This is easily understood by inspection of Fig. 12, showing d-values (and their coincidences) and intensities of the compounds in the system NiO–TiO_2. It is demonstrated in this paper that powder samples, especially if used in diffusion experiments or as calibration standards, must be judged with caution. Compounds in low concentrations can be masked on the surface of a crystal grain and cannot be analyzed by optical or even electron microprobe analyses. Exsolutions in powder

specimens will preferably gather on grain boundaries or surfaces where they may be overlooked, but they are visible if considerably large single crystals are used as starting material as shown for the NiO–TiO_2 single crystal diffusion couples.

Acknowledgments

Stimulating discussions with O. W. Flörke have provided much inspiration for this work. The author also thanks G. Bayer, O. W. Flörke, and H. D. Werner for supplying unpublished data, G. Hubert and H. Revcolevschi for help in growing NiO single crystals, K. Abraham for electron microprobe analyses, and P. Grosse and D. Leusmann for experimental advice. The author is grateful to O. W. Flörke, F. D. Bloss, and G. Lager for critical reading of the manuscript.

References

1. J. P. Wittke, *J. Electrochem. Soc.* **113**, 193 (1966).
2. R. D. Shannon and C. T. Prewitt, *Acta Crystallogr. B* **25**, 925 (1969).
3. H. Birnbaum and R. K. Scott, *J. Amer. Chem. Soc.* **72**, 1398 (1950).
4. W. N. Eremenko and A. M. Beinish, *Zh. Neorg. Chim.* **1**, 2119 (1956).
5. B. A. Loshkarev, N. A. Sycheva, and T. A. Ustyantseva, *Izv. Akad. Nauk. USSR Neorg. Mater.* **3**, 2040 (1967).
6. G. V. Klesheev and A. N. Sheinkman, "Miner. Pigmenty" (S.A. Shreiner, ed.), p. 29. Khiniya Leningrad Ofd., Leningrad (1970).
7. B. A. Loshkarev and N. A. Sycheva, *Russ. J. Inorg. Chem.* **15**, 8 (1970).
8. C. Macarovici and M. Zaharescu, *Rev. Roum. Chim.* **16**, 577 (1971).
9. L. M. Goldstein, I. I. Kalichenko, A. N. Sheinkman, and V. N. Turlakov, *Russ. J. Inorg. Chem.* **18**, 1694 (1973).
10. T. Satow, T. Isano, and T. Homma, *Nippon Kinzoku Gakkaishi* **38**, 242 (1974).
11. N. J. Barber and E. N. Farabaugh, *J. Appl. Phys.* **36**, 2803 (1965).
12. M. Zaharescu and C. Macarovici, *Rev. Roum. Chim.* **16**, 1323 (1971).
13. G. Bayer and O. W. Flörke, *Naturwissenschaften* **60**, 102 (1973).
14. H. D. Werner and W. Gebert, *N. Jb. Miner. Mh.* **1976**, 44 (1976).
15. Th. Armbruster, *Naturwissenschaften* **64**, 635 (1977).
16. W. Laqua, E. W. Schulz, and B. Reuter, *Z. Anorg. Allg. Chem.* **433**, 167 (1977).
17. F. Shimura and T. Kawamura, *Japan. J. Appl. Phys.* **15**, 1403 (1976).
18. M. Saurat and H. Revcolevschi, *Rev. Int. Hautes Temp. Refrac.* **8**, 291 (1971).
19. S. Kachi, K. Momiyama, and S. Shimizu, *J. Phys. Soc. Japan* **18**, 106 (1963).
20. R. K. Datta and R. Roy, *J. Amer. Ceram. Soc.* **50**, 578 (1967).
21. "International Tables for X-ray Crystallography," 3. ed., Vol. 1. Kynoch Press, Birmingham (1969).
22 C. Zeller, J. Hubsch, J. C. Reithler, and J. Bolfa, *C.R. Acad. Sci. Paris B* **264**, 1335 (1965).
23. E. W. Gorter, *Phillips Res. Rep.* **9**, 295 (1954).
24. I. I. Vishnevskii, G. G. Alapin, and V. N. Skripak, *Inorg. Mater.* **6**, 269 (1970).
25. P. Porta, F. S. Stone, and R. G. Turner, *J. Solid State Chem.* **11**, 135 (1974).
26. G. Marnier and J. Bolfa, *Bull. Soc. Franc. Miner. Cristallogr.* **98**, 260 (1975).
27. W. Laqua and B. Reuter, *J. Solid State Chem.* **9**, 24 (1974).
28. J. Mimkes and M. Wuttig, *Phys. Rev. B* **2**, 1619 (1970).
29. H. B. Huntington and G. A. Sullivan, *Phys. Rev. Lett.* **14**, 177 (1965).
30. T. S. Lundy and W. A. Coghlan, *J. Phys. Coll. Ser.* **8**, 34, C-9-299 (1973).
31. O. W. Flörke and Ch. W. Lee, *J. Solid State Chem.* **1**, 445 (1970).
32. L. A. Bursill, B. G. Hyde, and D. K. Philp, *Phil. Mag. Ser.* **8**, 23, 1501 (1971).